Available online at www.sciencedirect.com
SCIENCE DIRECT®
International Journal of Thermal Sciences 44 (2005) 787–798
International Journal of Thermal Sciences
www.elsevier.com/locate/ijts

Heat transfer in a laminar flow in a helical pipe filled with a fluid saturated porous medium

Liping Cheng, Andrey V. Kuznetsov *

Department of Mechanical and Aerospace Engineering, North Carolina State University, Campus Box 7910, Raleigh, NC 27695-7910, USA

Received 4 August 2004; received in revised form 10 December 2004; accepted 14 December 2004

Available online 7 April 2005

Abstract

This paper presents the first attempt to investigate numerically heat transfer in a helical pipe filled with a fluid saturated porous medium; the analysis is based on the full momentum equation for porous media that accounts for the Brinkman and Forchheimer extensions of the Darcy law as well as for the flow inertia. Numerical computations are performed in an orthogonal helical coordinate system. The effects of the Darcy number, the Forchheimer coefficient as well as the Dean and Germano numbers on the axial flow velocity, secondary flow, temperature distribution, and the Nusselt number are investigated.

Keywords: Heat transfer; Helical pipe; Porous medium; Laminar flow; Orthogonal helical coordinates

1. Introduction

The investigation of flows in porous media is motivated by various engineering applications, such as migration of moisture in fibrous insulation, grain storage, transport in contaminated soils, underground disposal of nuclear wastes, transport in drying processes, heat exchanges, etc. Nield and Bejan [1] summarized the state-of-art on this topic. Another quickly developing research field related to porous media is concerned with biomedical applications. In a clotted artery, the lesions or "plaques" within the artery wall consist of localized deposits of fat compounds (lipids) surrounded by cells recruited from the blood stream and scar tissue; this acts as a porous medium that may diminish or completely eliminate the blood flow. The coronary arteries surrounding the heart are curved and at least segments of them can be modeled as helical.

Flow in helical pipes is also a subject of intensive investigation. Of primary interest is the secondary flow caused by the centrifugal force in a helical pipe. Numerical studies have been conducted to examine the effects of torsion and curvature on the Newtonian fluid flow in helical pipes utilizing the Dean number, $Dn = \varepsilon^{1/2}Re$, and the Germano number, $Gn = (\varepsilon\lambda)Re$, to characterize the magnitude and the shape of the secondary flow and the effects of the curvature and torsion on helical pipe flow [2–9]. Sandeep et al. [10] extended the analysis of a helical pipe flow to non-Newtonian fluids; the numerical research was performed in a Cartesian coordinate system. Cheng and Kuznetsov [11] used the orthogonal helical coordinate system to study the effects of torsion and curvature on non-Newtonian fluid flow in helical pipes and compared the flow dynamics between Newtonian and non-Newtonian fluids.

Numerical computations of heat transfer in helical pipes were reported in a number of publications [12–16]. Cheng and Kuznetsov [17] studied heat transfer in a fully-developed laminar flow of a non-Newtonian fluid in a helical pipe with a constant wall heat flux; the effects of the Dean and Germano numbers with a fixed Reynolds number on the hydrodynamics and heat transfer in non-Newtonian fluid flow in helical pipes were investigated. Nield and Kuznetsov [18] presented a perturbation analysis and obtained an analytical expression for the Nusselt number in a helical pipe filled

* Corresponding author.
E-mail address: avkuznet@eos.ncsu.edu (A.V. Kuznetsov).

1290-0729/$ – see front matter
doi:10.1016/j.ijthermalsci.2004.12.009

Nomenclature

a	pipe radius	m
C_F	Forchheimer coefficient	
Da	Darcy number, K/a^2	
Dn	Dean number, $\varepsilon^{1/2}Re$	
Gn	Germano number, $\varepsilon\lambda\, Re$	
h_s	dimensionless scale factor	
$\tilde{h}_r$, $\tilde{h}_s$, $\tilde{h}_\theta$	dimensional scale factors	
k	thermal conductivity	$\mathrm{W\cdot m^{-1}\cdot K^{-1}}$
K	permeability	$\mathrm{m^2}$
Nu	Nusselt number, $\frac{2a}{k}\frac{q''_w}{(\tilde{T}_w-\tilde{T}_b)}$	
r	dimensionless radial coordinate, $\tilde{r}/a$	
$\tilde{r}$	radial coordinate	m
$\hat{\mathbf{r}}$	residual vector	
Re	Reynolds number, $\rho_f U a/\mu$	
s	dimensionless axial coordinate, $\tilde{s}/a$	
$\tilde{s}$	axial coordinate	m
p	pitch	m
P	dimensionless pressure, $\widetilde{P}/\rho U^2$	
$\widetilde{P}$	pressure	Pa
Pr	Prandtl number, $c_p\mu/k_m$	
T	dimensionless temperature, defined in Eq. (10)	
$\widetilde{T}$	temperature	K
$\widetilde{T}_b$	mean temperature, defined in Eq. (10)	K
$\widetilde{T}_w$	wall temperature	K
U	mean velocity, defined in Eq. (10)	$\mathrm{m\cdot s^{-1}}$
$\tilde{\mathbf{v}}$	velocity vector	$\mathrm{m\cdot s^{-1}}$
u_s, u_r, u_θ	dimensionless velocity components, $\tilde{u}_s/U, \tilde{u}_r/U, \tilde{u}_\theta/U$	
$\tilde{u}_s, \tilde{u}_r, \tilde{u}_\theta$	velocity components	$\mathrm{m\cdot s^{-1}}$

Greek symbols

ε	dimensionless curvature, κa	
θ	angle, defined in Fig. 1(b)	
κ	curvature	$\mathrm{m^{-1}}$
λ	the ratio of torsion to curvature, τ/κ	
μ	effective dynamic viscosity of a porous medium	$\mathrm{kg\cdot m^{-1}\cdot s^{-1}}$
ν	effective kinematic viscosity of a porous medium	$\mathrm{m^2\cdot s^{-1}}$
ξ	angle, defined in Eq. (11)	
ρ_f	fluid density	$\mathrm{kg\cdot m^{-3}}$
τ	torsion	$\mathrm{m^{-1}}$
φ	porosity	
ϕ	angle, defined in Fig. 1(b)	

Subscripts

s	axial direction
r	radial direction
θ	circumferential direction

with a porous medium for the case when the flow in a pipe is described by the Darcy law.

In the previous paper, Cheng and Kuznetsov [19] investigated laminar flow in a helical pipe filled with a porous medium utilizing the Brinkman–Forchheimer-extended Darcy equation with inertia terms. The purpose of this paper is to perform numerical simulations of heat transfer for a fully developed laminar flow of a Newtonian fluid in a helical pipe filled with a fluid saturated porous medium subjected to a constant wall heat flux. An orthogonal helical coordinate system is utilized. The effects of the Darcy number, the Forchheimer coefficient, the Dean number, and the Germano number with a fixed Reynolds number on the hydrodynamics and heat transfer in helical pipes are investigated.

2. Governing equations

A helical pipe (Fig. 1(a)) is characterized by two parameters, the curvature, κ, and the torsion, τ, which are defined as, respectively

$$\kappa = \frac{R}{R^2+p^2}, \qquad \tau = \frac{p}{R^2+p^2} \tag{1}$$

An orthogonal helical coordinate system introduced by Germano [3,4] is utilized with a helical coordinate s for the axial direction, r for the radial direction, and θ for the circumferential direction (Fig. 1(b)). The continuity and momentum equations in the vector form are

$$\nabla\cdot\tilde{\mathbf{v}} = 0 \tag{2}$$

and

$$\frac{\rho_f}{\varphi^2}(\tilde{\mathbf{v}}\cdot\nabla)\tilde{\mathbf{v}} = -\nabla\widetilde{P} + \frac{\mu}{\varphi}\nabla^2\tilde{\mathbf{v}} - \frac{\mu}{K}\tilde{\mathbf{v}} - \frac{C_F\rho_f}{K^{1/2}}|\tilde{\mathbf{v}}|\tilde{\mathbf{v}} \tag{3}$$

where K is the permeability of the porous medium (which is assumed to be isotropic with a uniform porosity), C_F is the Forchheimer coefficient (which, for a given geometry of a porous matrix, is a dimensionless form-drag constant [1]), and φ is the porosity.

Eq. (3) is a full momentum equation for the steady flow in porous media that accounts for the Brinkman and Forchheimer extensions of the Darcy law as well as for the flow inertia [1].

The energy equation (the effect of thermal dispersion is neglected) is given by

$$(\rho c_p)_f\frac{D\widetilde{T}}{Dt} = \nabla\cdot\left[k_m\nabla\widetilde{T}\right] \tag{4}$$

$$k_m = \varphi k_f + (1-\varphi)k_s \tag{5}$$

where k_m is the effective thermal conductivity of porous medium and the subscripts 'f' and 's' refer to 'fluid' and

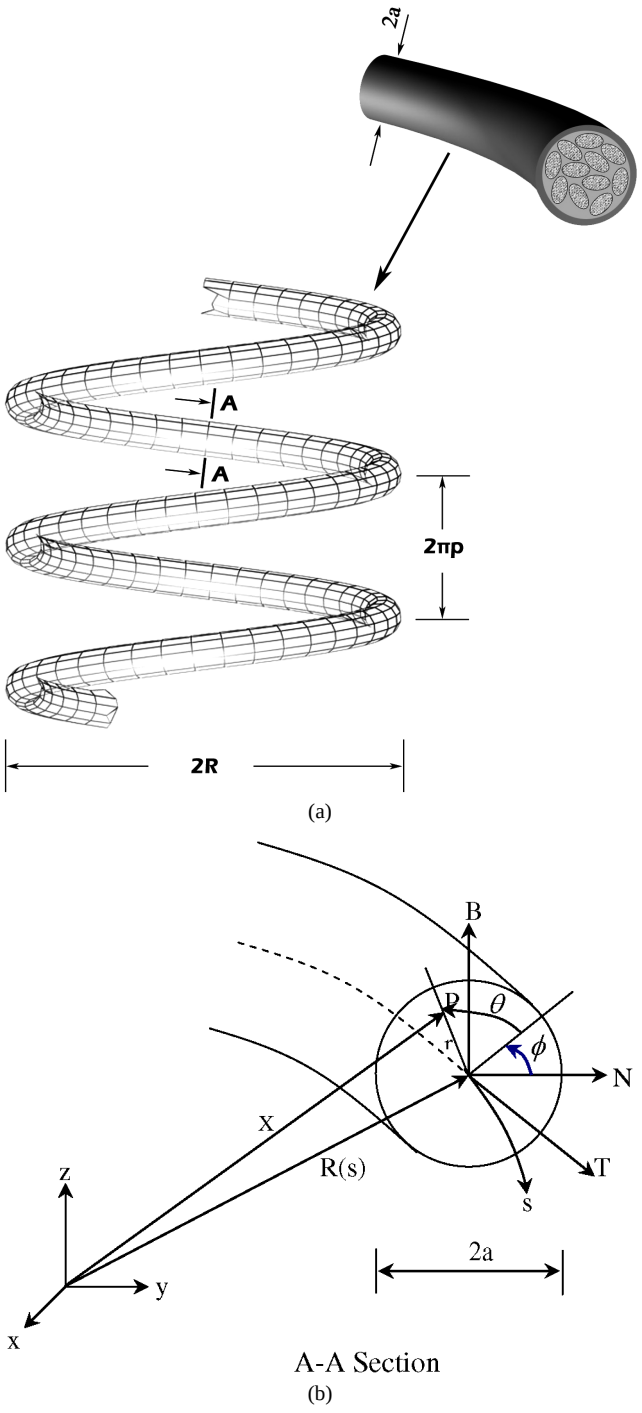

Fig. 1. (a) Schematic diagram of a helical pipe. (b) The orthogonal helical coordinate system.

'solid', respectively. Eq. (5) is a commonly used approximation for porous media [1]. In the orthogonal helical coordinate system, the scale factors are given by

$$\tilde{h}_s = 1 + \kappa\tilde{r}\sin(\theta+\phi), \qquad \tilde{h}_r = 1, \qquad \tilde{h}_\theta = \tilde{r} \tag{6}$$

The dimensionless governing equations for the flow in a porous medium written in the orthogonal helical coordinate system are the continuity equation

$$\frac{\partial(ru_s)}{\partial s} + \frac{\partial(rh_s u_r)}{\partial r} + \frac{\partial(h_s u_\theta)}{\partial\theta} = 0 \tag{7}$$

the momentum equations

$$\begin{aligned}
&\frac{1}{\varphi^2}\frac{1}{h_s r}\left(\frac{\partial(ru_s u_s)}{\partial s} + \frac{\partial(rh_s u_r u_s)}{\partial r} + \frac{\partial(h_s u_\theta u_s)}{\partial\theta}\right)\\
&\quad + \frac{1}{\varphi^2}\frac{\varepsilon}{h_s}u_s\big(u_r\sin(\theta+\phi) + u_\theta\cos(\theta+\phi)\big)\\
&\quad = -\frac{1}{h_s}\frac{\partial P}{\partial s} + \frac{1}{\varphi}\frac{1}{Re}\left\{\frac{1}{h_s}\frac{\partial}{\partial s}\left[\frac{1}{h_s r}\left[\frac{\partial(ru_s)}{\partial s}\right.\right.\right.\\
&\quad \left.\left.\left. + \frac{\partial(rh_s u_r)}{\partial r} + \frac{\partial(h_s u_\theta)}{\partial\theta}\right]\right]\right.\\
&\quad - \frac{1}{r}\left(\frac{\partial}{\partial r}\left(\frac{r}{h_s}\left(\frac{\partial u_r}{\partial s} - \frac{\partial}{\partial r}(h_s u_s)\right)\right)\right.\\
&\quad \left.\left. - \frac{\partial}{\partial\theta}\left(\frac{1}{h_s r}\left(\frac{\partial}{\partial\theta}(h_s u_s) - \frac{\partial}{\partial\theta}(ru_\theta)\right)\right)\right)\right\}\\
&\quad - \frac{1}{Re}\frac{1}{Da}u_s - \frac{C_F}{Da^{1/2}}u_s\big(u_s^2+u_r^2+u_\theta^2\big)^{1/2}
\end{aligned} \tag{8a}$$

$$\begin{aligned}
&\frac{1}{\varphi^2}\frac{1}{h_s r}\left(\frac{\partial(ru_s u_r)}{\partial s} + \frac{\partial(rh_s u_r u_r)}{\partial r} + \frac{\partial(h_s u_\theta u_r)}{\partial\theta}\right)\\
&\quad - \frac{1}{\varphi^2}\frac{u_\theta^2}{r} - \frac{1}{\varphi^2}\frac{\varepsilon}{h_s}u_s^2\sin(\theta+\phi)\\
&\quad = -\frac{\partial P}{\partial r} + \frac{1}{\varphi}\frac{1}{Re}\left\{\frac{\partial}{\partial r}\left[\frac{1}{h_s r}\left[\frac{\partial(ru_s)}{\partial s}\right.\right.\right.\\
&\quad \left.\left.\left. + \frac{\partial(rh_s u_r)}{\partial r} + \frac{\partial(h_s u_\theta)}{\partial\theta}\right]\right]\right.\\
&\quad - \frac{1}{h_s r}\left(\frac{\partial}{\partial\theta}\left(\frac{h_s}{r}\left(\frac{\partial}{\partial r}(ru_\theta) - \frac{\partial u_r}{\partial\theta}\right)\right)\right.\\
&\quad \left.\left. - \frac{\partial}{\partial s}\left(\frac{r}{h_s}\left(\frac{\partial u_r}{\partial s} - \frac{\partial}{\partial r}(h_s u_s)\right)\right)\right)\right\}\\
&\quad - \frac{1}{Re}\frac{1}{Da}u_r - \frac{C_F}{Da^{1/2}}u_r\big(u_s^2+u_r^2+u_\theta^2\big)^{1/2}
\end{aligned} \tag{8b}$$

$$\begin{aligned}
&\frac{1}{\varphi^2}\frac{1}{h_s r}\left(\frac{\partial(ru_s u_\theta)}{\partial s} + \frac{\partial(rh_s u_r u_\theta)}{\partial r} + \frac{\partial(h_s u_\theta u_\theta)}{\partial\theta}\right)\\
&\quad - \frac{1}{\varphi^2}\frac{\varepsilon}{h_s}u_s^2\cos(\theta+\phi) + \frac{1}{\varphi^2}\frac{u_r u_\theta}{r}\\
&\quad = -\frac{1}{r}\frac{\partial P}{\partial\theta} + \frac{1}{\varphi}\frac{1}{Re}\left\{\frac{1}{r}\frac{\partial}{\partial\theta}\left[\frac{1}{h_s r}\left[\frac{\partial(ru_s)}{\partial s}\right.\right.\right.\\
&\quad \left.\left.\left. + \frac{\partial(rh_s u_r)}{\partial r} + \frac{\partial(h_s u_\theta)}{\partial\theta}\right]\right]\right.\\
&\quad - \frac{1}{h_s}\left(\frac{\partial}{\partial s}\left(\frac{1}{h_s r}\left(\frac{\partial}{\partial\theta}(h_s u_s) - \frac{\partial}{\partial s}(ru_\theta)\right)\right)\right.\\
&\quad \left.\left. - \frac{\partial}{\partial r}\left(\frac{h_s}{r}\left(\frac{\partial}{\partial r}(ru_\theta) - \frac{\partial u_r}{\partial\theta}\right)\right)\right)\right\}\\
&\quad - \frac{1}{Re}\frac{1}{Da}u_\theta - \frac{C_F}{Da^{1/2}}u_\theta\big(u_s^2+u_r^2+u_\theta^2\big)^{1/2}
\end{aligned} \tag{8c}$$

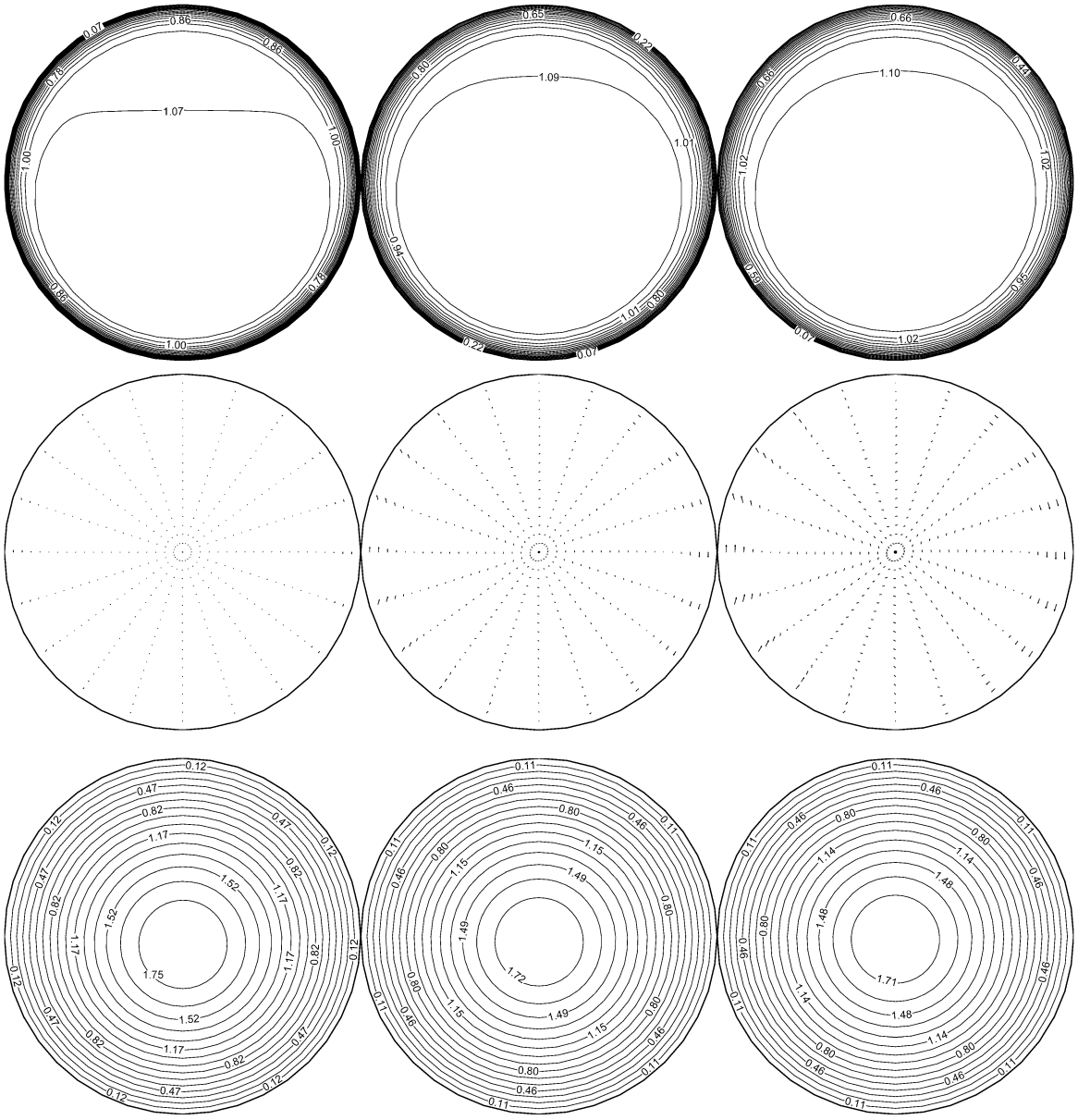

Fig. 2. Contour lines of the axial velocity (top), vector plots of the secondary flow (middle) and contour lines of the dimensionless temperature (bottom) at $Re = 100$, $C_F = 0.55$, $\varphi = 0.95$, $\varepsilon = 0.1$, $\lambda = 0.1$, $Dn = 31.6$, $Gn = 1.0$ for different values of the Darcy number: (a) $Da = 10^{-2}$; (b) $Da = 5 \times 10^{-2}$; (c) $Da = 10^{-1}$.

and the energy equation

$$\left(\frac{\partial(ru_sT)}{\partial s} + \frac{\partial(rh_su_rT)}{\partial r} + \frac{\partial(h_su_\theta T)}{\partial \theta}\right) = \frac{ru_s}{RePr} + \frac{1}{RePr}\left(\frac{\partial}{\partial s}\left[\frac{r}{h_s}\frac{\partial T}{\partial s}\right] + \frac{\partial}{\partial r}\left[h_s r\frac{\partial T}{\partial r}\right] + \frac{\partial}{\partial \xi}\left[\frac{h_s}{r}\frac{\partial T}{\partial \theta}\right]\right) \tag{9}$$

where

$$s = \frac{\tilde{s}}{a}, \qquad r = \frac{\tilde{r}}{a}, \qquad (u_s, u_r, u_\theta) = \left(\frac{\tilde{u}_s}{U}, \frac{\tilde{u}_r}{U}, \frac{\tilde{u}_\theta}{U}\right)$$

$$P = \frac{\widetilde{P}}{\rho_f U^2}, \qquad \varepsilon = \kappa a, \qquad \lambda = \frac{\tau}{\kappa}$$

$$Re = \frac{\rho_f U a}{\mu}, \qquad Da = \frac{K}{a^2}$$

$$U = \frac{1}{\pi}\int_0^{2\pi}\int_0^1 \tilde{u}_s r \,\mathrm{d}r\,\mathrm{d}\theta, \qquad \widetilde{T}_b = \frac{1}{U\pi}\int_0^{2\pi}\int_0^1 \tilde{u}_s \widetilde{T} r \,\mathrm{d}r\,\mathrm{d}\theta$$

$$Pr = \frac{c_p\mu}{k_m}, \qquad Nu = \frac{2a}{k}\frac{q''_w}{(\widetilde{T}_w - \widetilde{T}_b)}$$

$$T = \frac{\widetilde{T} - \widetilde{T}_w}{Nu(\widetilde{T}_b - \widetilde{T}_w)} \tag{10}$$

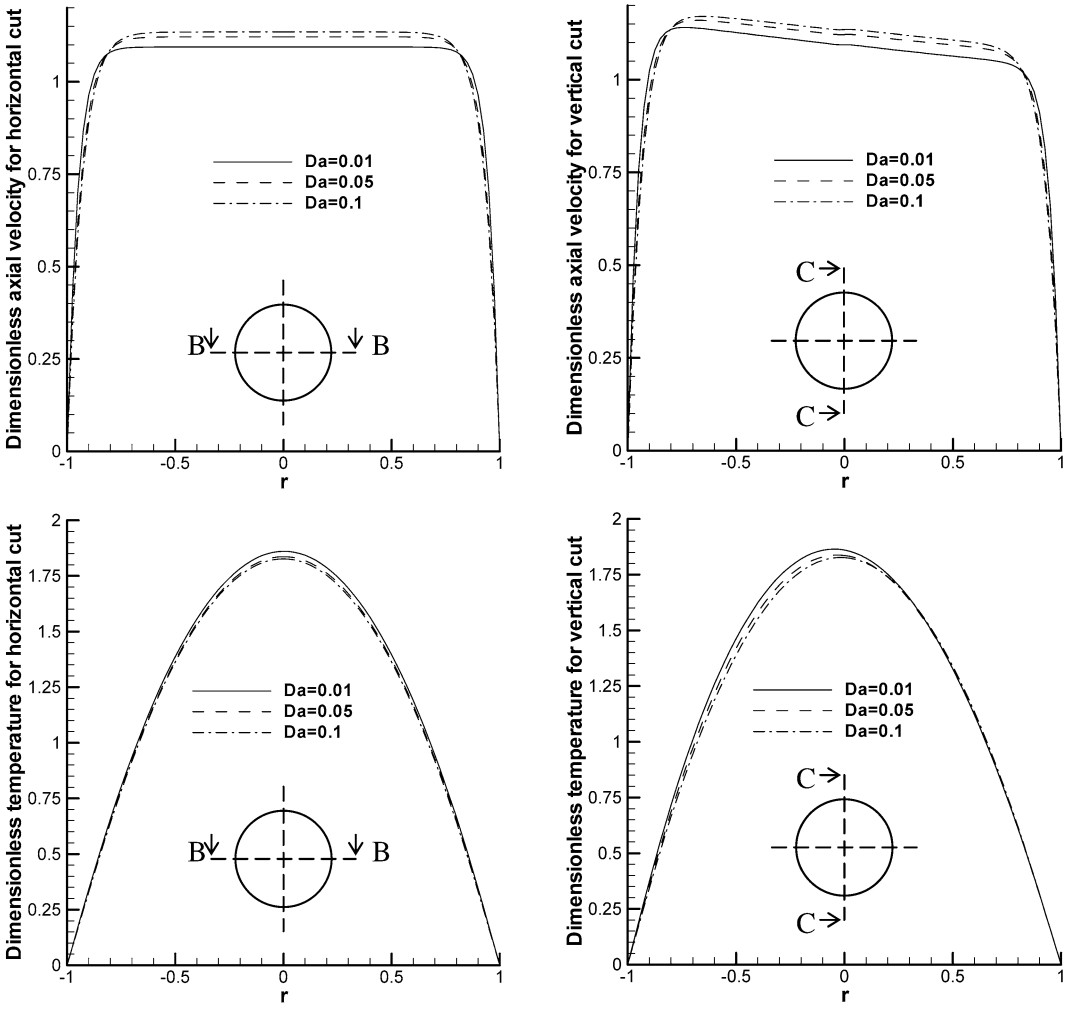

Fig. 3. Profile plots of the dimensionless axial velocity and dimensionless temperature in the horizontal and vertical cut view of the pipe at $Re = 100$, $C_F = 0.55$, $\varphi = 0.95$, $\varepsilon = 0.1$, $\lambda = 0.1$, $Dn = 31.6$, $Gn = 1.0$ for different values of the Darcy number: (a) $Da = 10^{-2}$; (b) $Da = 5 \times 10^{-2}$; (c) $Da = 10^{-1}$.

where a is the radius of the pipe and U is the mean velocity defined in Eq. (10).

A fully developed laminar flow is considered so that the dynamic variables except for the pressure are independent of s; therefore, the following simplifying transformation is performed from s, r, θ to s, r, ξ:

$$\theta + \phi \Longrightarrow \xi, \qquad \frac{\partial}{\partial s} \Longrightarrow \frac{\partial}{\partial s} - \varepsilon\lambda\frac{\partial}{\partial \xi}$$
$$\frac{\partial}{\partial \theta} \Longrightarrow \frac{\partial}{\partial \xi} \tag{11}$$

The governing equations are then reduced as:

$$-\varepsilon\lambda\frac{\partial(ru_s)}{\partial \xi} + \frac{\partial(rh_s u_r)}{\partial r} + \frac{\partial(h_s u_\theta)}{\partial \xi} = 0 \tag{12}$$

$$\frac{1}{\varphi^2}\frac{1}{h_s r}\left(-\varepsilon\lambda\frac{\partial(ru_s u_s)}{\partial \xi} + \frac{\partial(rh_s u_r u_s)}{\partial r} + \frac{\partial(h_s u_\theta u_s)}{\partial \xi}\right) + \frac{1}{\varphi^2}\frac{\varepsilon}{h_s}u_s(u_r \sin\xi + u_\theta \cos\xi)$$
$$= -\frac{1}{h_s}\left(\frac{\partial P}{\partial s} - \varepsilon\lambda\frac{\partial P}{\partial \xi}\right) + \frac{1}{\varphi}\frac{1}{Re}\left\{-\varepsilon\lambda\frac{1}{h_s}\frac{\partial}{\partial \xi}\left[\frac{1}{h_s r}\left[-\varepsilon\lambda\frac{\partial(ru_s)}{\partial \xi} + \frac{\partial(rh_s u_r)}{\partial r} + \frac{\partial(h_s u_\theta)}{\partial \xi}\right]\right] - \frac{1}{r}\left(\frac{\partial}{\partial r}\left(\frac{r}{h_s}\left(-\varepsilon\lambda\frac{\partial u_r}{\partial \xi} - \frac{\partial}{\partial r}(h_s u_s)\right)\right) - \frac{\partial}{\partial \xi}\left(\frac{1}{h_s r}\left(\frac{\partial}{\partial \xi}(h_s u_s) + \varepsilon\lambda\frac{\partial}{\partial \xi}(ru_\theta)\right)\right)\right)\right\} - \frac{1}{Re}\frac{1}{Da}u_s - \frac{C_F}{Da^{1/2}}u_s\left(u_s^2 + u_r^2 + u_\theta^2\right)^{1/2} \tag{13a}$$

$$\frac{1}{\varphi^2}\frac{1}{h_s r}\left(-\varepsilon\lambda\frac{\partial(ru_s u_r)}{\partial \xi} + \frac{\partial(rh_s u_r u_r)}{\partial r} + \frac{\partial(h_s u_\theta u_r)}{\partial \xi}\right) - \frac{1}{\varphi^2}\frac{u_\theta^2}{r} - \frac{1}{\varphi^2}\frac{\varepsilon}{h_s}u_s^2 \sin\xi$$
$$= -\frac{\partial P}{\partial r} + \frac{1}{\varphi}\frac{1}{Re}\left\{\frac{\partial}{\partial r}\left[\frac{1}{h_s r}\left[-\varepsilon\lambda\frac{\partial(ru_s)}{\partial \xi}\right.\right.\right.$$

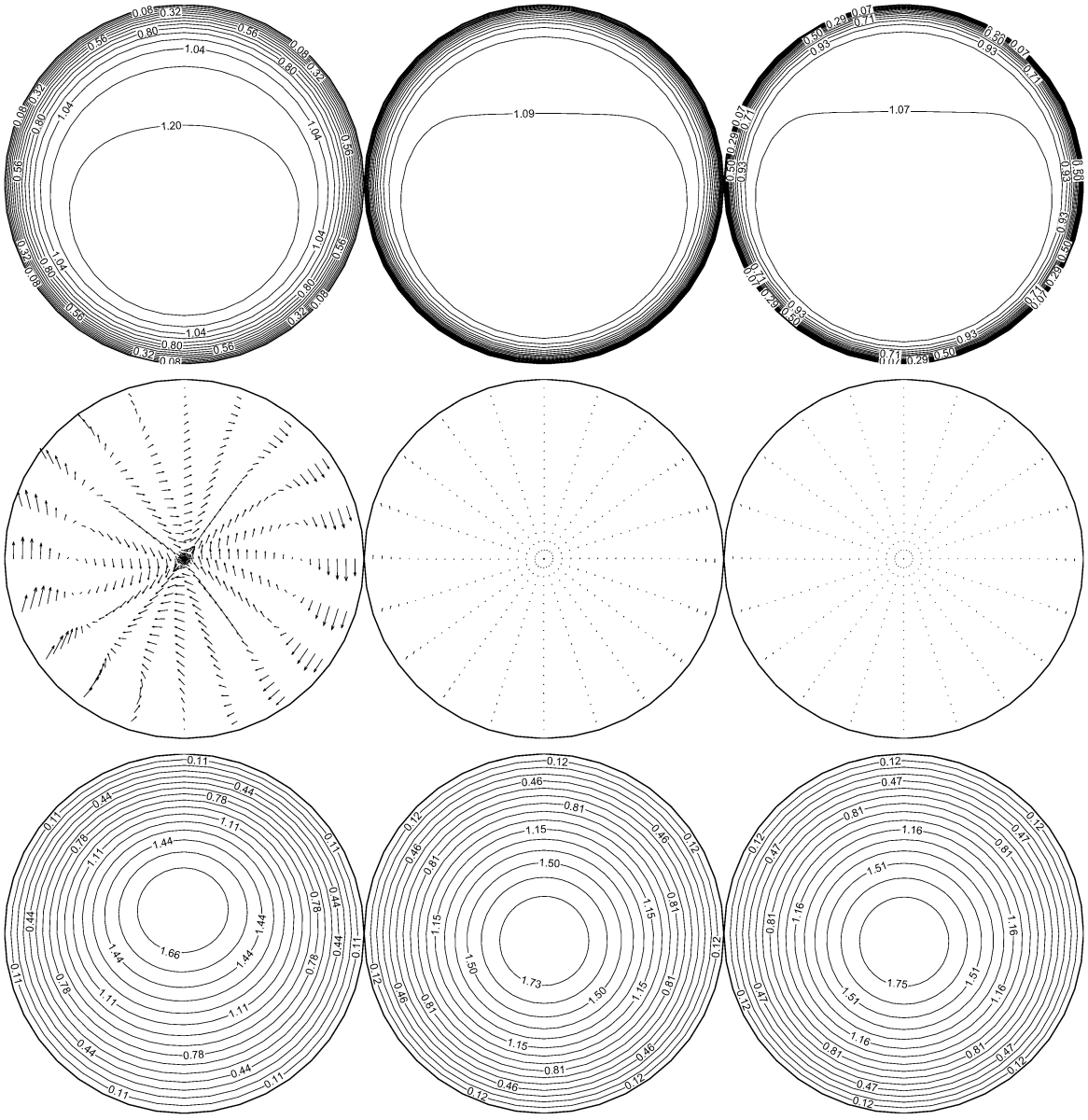

Fig. 4. Contour lines of the axial velocity (top), vector plots of the secondary flow (middle), and contour lines of the dimensionless temperature (bottom) at $Re = 100$, $Da = 10^{-2}$, $\varphi = 0.95$, $\varepsilon = 0.1$, $\lambda = 0.1$, $Dn = 31.6$, $Gn = 1.0$ for different values of the Forchheimer coefficient: (a) $C_F = 0.0$; (b) $C_F = 0.25$; (c) $C_F = 0.50$.

$$+\frac{\partial(rh_s u_r)}{\partial r}+\frac{\partial(h_s u_\theta)}{\partial \xi}\Bigg]\Bigg]$$
$$-\frac{1}{h_s r}\left(\frac{\partial}{\partial \xi}\left(\frac{h_s}{r}\left(\frac{\partial}{\partial r}(ru_\theta)-\frac{\partial u_r}{\partial \xi}\right)\right)\right.$$
$$\left.+\varepsilon\lambda\frac{\partial}{\partial \xi}\left(\frac{r}{h_s}\left(-\varepsilon\lambda\frac{\partial u_r}{\partial \xi}-\frac{\partial}{\partial r}(h_s u_s)\right)\right)\right)\Bigg\}$$
$$-\frac{1}{Re}\frac{1}{Da}u_r-\frac{C_F}{Da^{1/2}}u_r\left(u_s^2+u_r^2+u_\theta^2\right)^{1/2} \qquad (13b)$$

$$\frac{1}{\varphi^2}\frac{1}{h_s r}\left(-\varepsilon\lambda\frac{\partial(ru_s u_\theta)}{\partial \xi}+\frac{\partial(rh_s u_r u_\theta)}{\partial r}+\frac{\partial(h_s u_\theta u_\theta)}{\partial \xi}\right)$$
$$-\frac{1}{\varphi^2}\frac{\varepsilon}{h_s}u_s^2\cos\xi+\frac{1}{\varphi^2}\frac{u_r u_\theta}{r}$$
$$=-\frac{1}{r}\frac{\partial P}{\partial \xi}+\frac{1}{\varphi}\frac{1}{Re}\left\{\frac{1}{r}\frac{\partial}{\partial \xi}\left[\frac{1}{h_s r}\left[-\varepsilon\lambda\frac{\partial(ru_s)}{\partial \xi}\right.\right.\right.$$
$$\left.+\frac{\partial(rh_s u_r)}{\partial r}+\frac{\partial(h_s u_\theta)}{\partial \xi}\right]\Bigg]$$
$$-\frac{1}{h_s}\left(-\varepsilon\lambda\frac{\partial}{\partial \xi}\left(\frac{1}{h_s r}\left(\frac{\partial}{\partial \xi}(h_s u_s)+\varepsilon\lambda\frac{\partial}{\partial \xi}(ru_\theta)\right)\right)\right.$$
$$\left.\left.-\frac{\partial}{\partial r}\left(\frac{h_s}{r}\left(\frac{\partial}{\partial r}(ru_\theta)-\frac{\partial}{\partial \xi}(u_r)\right)\right)\right)\right\}$$
$$-\frac{1}{Re}\frac{1}{Da}u_\theta-\frac{C_F}{Da^{1/2}}u_\theta\left(u_s^2+u_r^2+u_\theta^2\right)^{1/2} \qquad (13c)$$

$$\left(-\varepsilon\lambda\frac{\partial(ru_s T)}{\partial \xi}+\frac{\partial(rh_s u_r T)}{\partial r}+\frac{\partial(h_s u_\theta T)}{\partial \xi}\right)$$

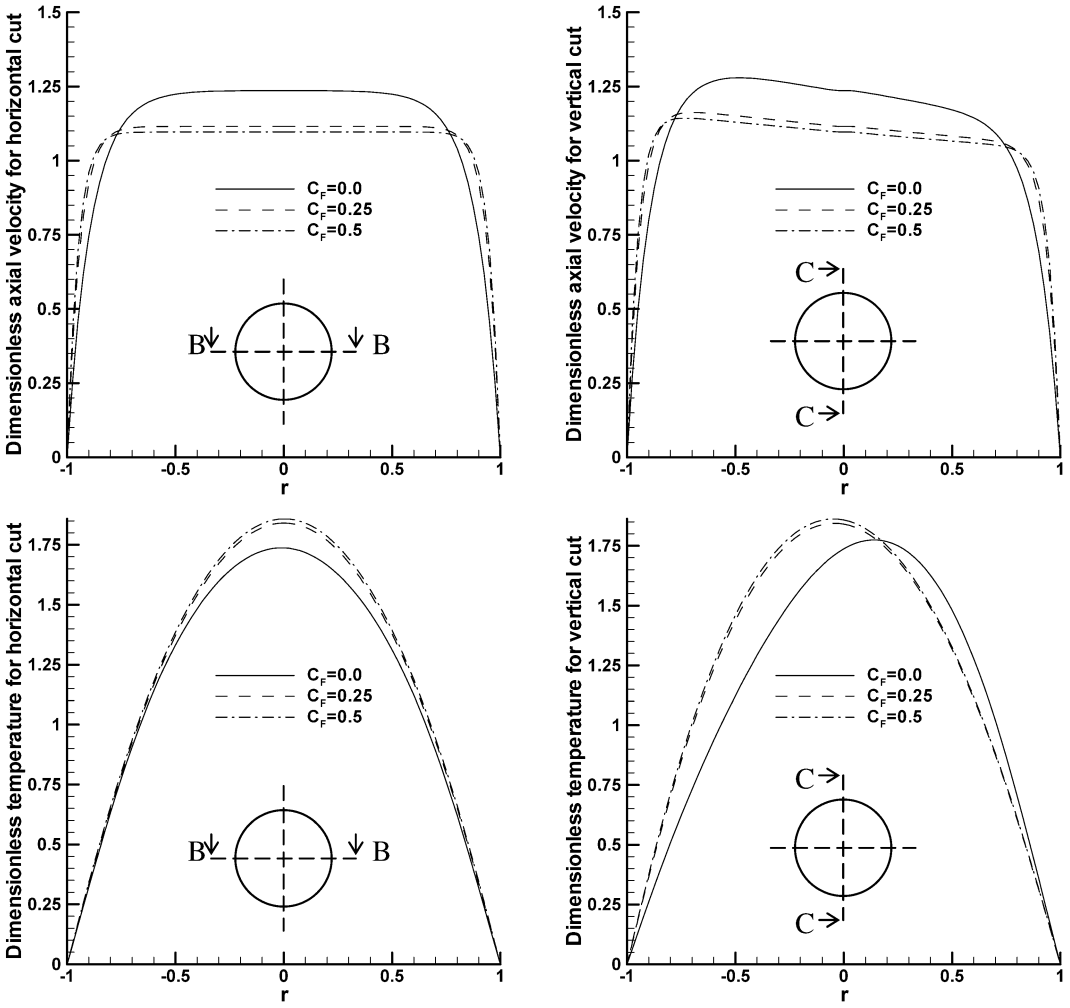

Fig. 5. Profile plots of the dimensionless axial velocity and dimensionless temperature in the horizontal and vertical cut view of the pipe at $Re = 100$, $Da = 10^{-2}$, $\varphi = 0.95$, $\varepsilon = 0.1$, $\lambda = 0.1$, $Dn = 31.6$, $Gn = 1.0$ for different values of the Forchheimer coefficient: (a) $C_F = 0.0$; (b) $C_F = 0.25$; (c) $C_F = 0.50$.

$$= \frac{ru_s}{Re\,Pr} + \frac{1}{Re\,Pr}\left((\varepsilon\lambda)^2\frac{\partial}{\partial\xi}\left[\frac{r}{h_s}\frac{\partial T}{\partial\xi}\right] + \frac{\partial}{\partial r}\left[h_s r\frac{\partial T}{\partial r}\right] + \frac{\partial}{\partial\xi}\left[\frac{h_s}{r}\frac{\partial T}{\partial\xi}\right]\right) \tag{14}$$

3. Computational procedure

A control volume-based finite difference method is utilized on an evenly spaced mesh in both radial and circumferential directions. The convection–diffusion terms are discretized with the power-law scheme (Patankar [20]) and the other terms are approximated by central differences. The SIMPLE algorithm (Patankar [20]) is adopted on a staggered grid arrangement to solve the governing equations.

A no-slip boundary condition is assumed at the walls of the helical pipe. To solve the numerical singularity at the pipe axis ($r = 0$), boundary values are needed for flow quantities, which are either located directly at the pipe axis or at the opposite sides of the pipe axis (Hüttl [7]; Cheng and Kuznetsov [11]). An initial value of the Reynolds number, which is needed to start the iterations, is estimated as follows. The flow is driven by a constant pressure gradient $\mathrm{d}P/\mathrm{d}s$ that has to balance the fluid friction in a porous medium, which implies that approximately (neglecting the Forchheimer resistance) the following equation is satisfied:

$$\left(\frac{\mathrm{d}P}{\mathrm{d}s}\right) = \frac{1}{Da\,Re} \tag{15}$$

This is used to evaluate only the initial value of *Re*. During the iteration process, *Re* is evaluated according to Eq. (10) utilizing the value of the mean velocity from the previous iteration.

A constant wall heat flux is assumed as the boundary condition for the energy equation. Since the effective dynamic viscosity of the porous medium is temperature-independent, the energy equation is solved after the velocity profile has been obtained. The effects of different parameters for the same values of the Reynolds number on the hydrodynamics and heat transfer in a helical pipe are investigated.

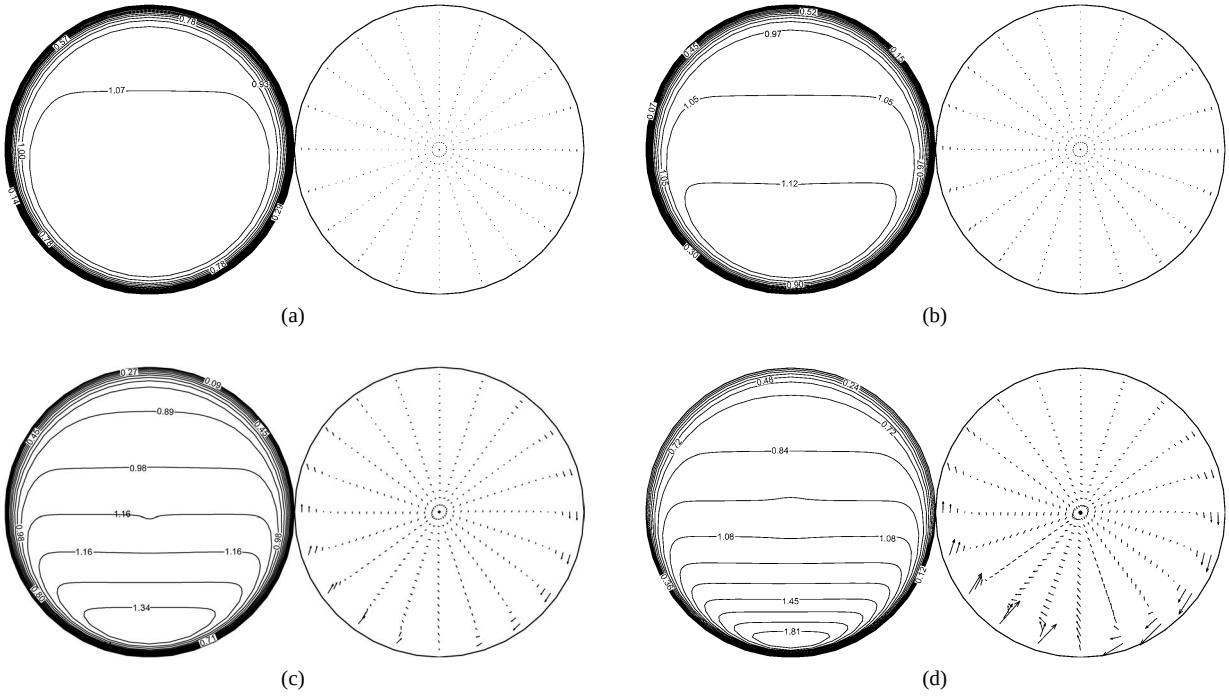

Fig. 6. Contour lines of the axial velocity (left) and vector plots of the secondary flow (right) at $Re = 100$, $Da = 10^{-2}$ $C_F = 0.55$, $\varphi = 0.95$, $Gn = 1.0$ for different values of the Dean number: (a) $\varepsilon = 0.1$, $\lambda = 0.1$, $Dn = 31.6$; (b) $\varepsilon = 0.2$, $\lambda = 0.05$, $Dn = 44.7$; (c) $\varepsilon = 0.5$, $\lambda = 0.02$, $Dn = 70.7$; (d) $\varepsilon = 0.8$, $\lambda = 0.0125$, $Dn = 89.4$.

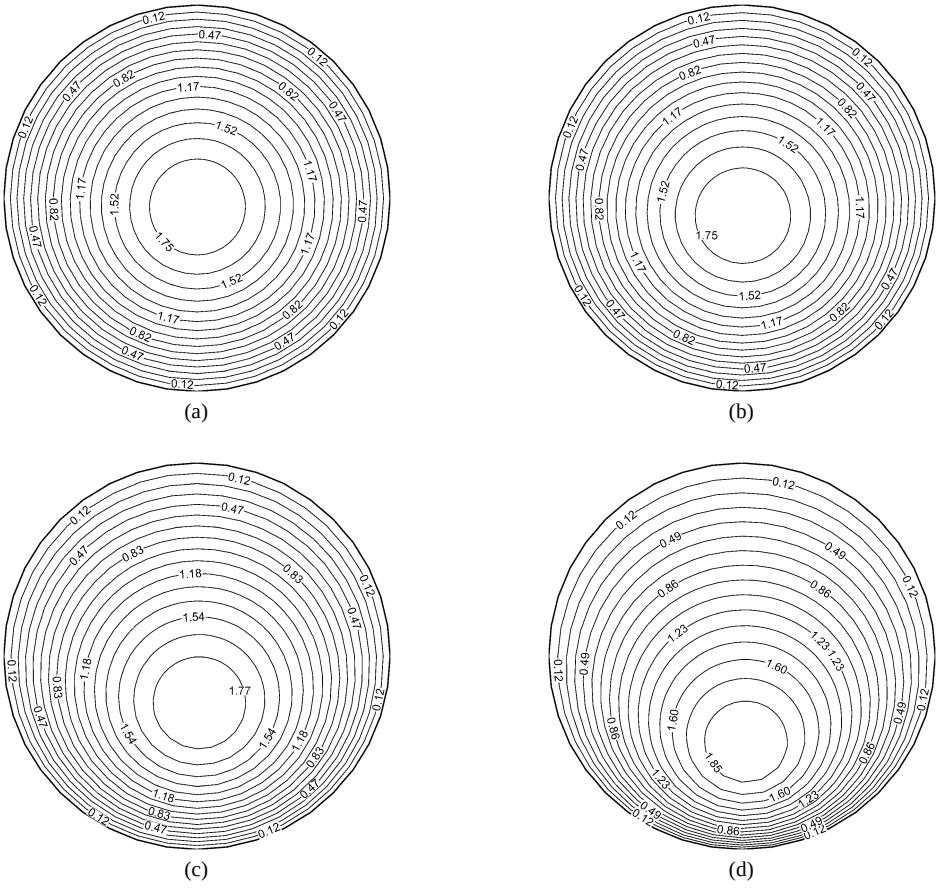

Fig. 7. Contour lines of the dimensionless temperature at $Re = 100$, $Da = 10^{-2}$, $C_F = 0.55$, $\varphi = 0.95$, $Gn = 1.0$ for different values of the Dean number: (a) $\varepsilon = 0.1$, $\lambda = 0.1$, $Dn = 31.6$; (b) $\varepsilon = 0.2$, $\lambda = 0.05$, $Dn = 44.7$; (c) $\varepsilon = 0.5$, $\lambda = 0.02$, $Dn = 70.7$; (d) $\varepsilon = 0.8$, $\lambda = 0.05$, $Dn = 89.4$.

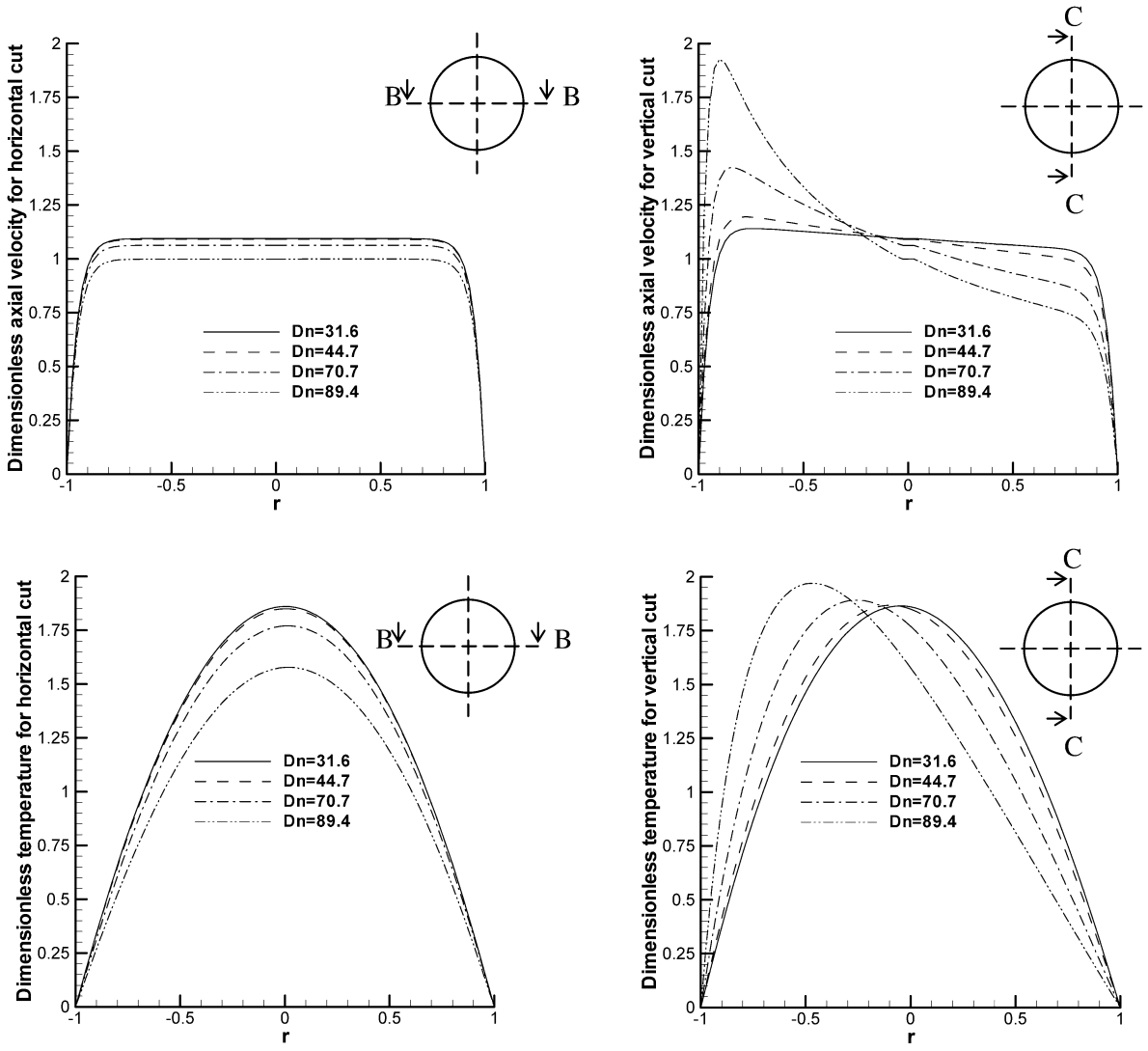

Fig. 8. Profile plot of the axial velocity and the dimensionless temperature in the horizontal and vertical cut view of the pipe at $Re = 100$, $Da = 10^{-2}$, $C_F = 0.55$, $\varphi = 0.95$, $Gn = 1.0$ for different values of the Dean number: (a) $\varepsilon = 0.1$, $\lambda = 0.1$, $Dn = 31.6$; (b) $\varepsilon = 0.2$, $\lambda = 0.05$, $Dn = 44.7$; (c) $\varepsilon = 0.5$, $\lambda = 0.02$, $Dn = 70.7$; (d) $\varepsilon = 0.8$, $\lambda = 0.0125$, $Dn = 89.4$.

4. Results and discussion

A constant Reynolds number of 100 is assumed for all cases to compare the effects of the Darcy number, the Forchheimer coefficient, the Dean number, and the Germano number. Values of the Nusselt number for different cases are listed in Table 1 to compare the heat transfer efficiency for different parameter values.

Figs. 2 and 3 show the effect of the Darcy number on the flow and heat transfer in a helical pipe. Fig. 2 depicts the axial velocity contours, velocity vector plot of the secondary flow and the dimensionless temperature contours for different Darcy numbers. This figure shows that with the increase of the Darcy number, the maximum of the axial velocity increases and the secondary flow becomes stronger. This is explained by a larger filtration velocity that can be attributed to a larger permeability for larger Darcy numbers. However, the dimensionless temperature decreases with the Darcy number, as shown in Fig. 2, and the Nusselt number becomes smaller, as shown in Table 1. The displacement of the maximum value of the axial velocity to the wall is apparent and can be explained by the effect of the centrifugal force in a helical pipe, but this does not happen for the dimensionless temperature, which remains parabolic for all computed values of the Darcy number. These trends can also be observed from the profile plots of the dimensionless axial velocity and temperature in the horizontal and vertical cut views of the cross section of the pipe (Fig. 3).

The effect of the Forchheimer coefficient, C_F, on the fluid flow and heat transfer in a helical pipe filled with a porous medium is shown in Figs. 4 and 5. The contour lines of the axial velocity show that the value of the maximum axial velocity decreases when C_F is increased and the profile plots of the axial velocity show that increas-

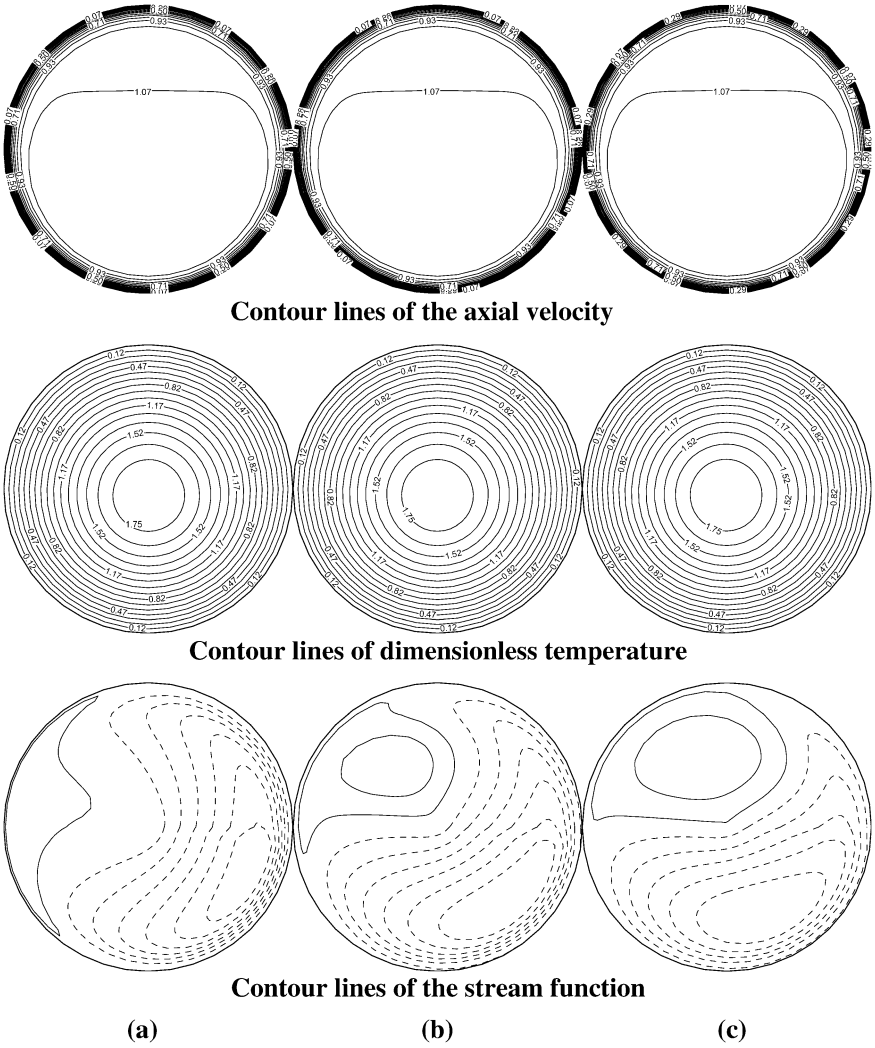

Fig. 9. Contour lines of the axial velocity, the dimensionless temperature and the stream function at $Re = 100$, $Da = 10^{-2}$, $C_F = 0.55$, $\varphi = 0.95$, $\varepsilon = 0.1$, $Dn = 31.6$ for different values of the Germano number: (a) $\lambda = 0.1$, $Gn = 1.0$; (b) $\lambda = 0.5$, $Gn = 5.0$; (c) $\lambda = 1.0$, $Gn = 10.0$.

Table 1
Nusselt number for different parameters

Da	C_F	ε	λ	Dn	Gn	Nu
0.01	0.55	0.10	0.10	31.60	1.00	21.10
0.05	0.55	0.10	0.10	31.60	1.00	12.40
0.10	0.55	0.10	0.10	31.60	1.00	10.19
0.01	0.00	0.10	0.10	31.60	1.00	6.34
0.01	0.25	0.10	0.10	31.60	1.00	15.34
0.01	0.50	0.10	0.10	31.60	1.00	20.30
0.01	0.55	0.10	0.10	31.60	1.00	21.13
0.01	0.55	0.20	0.05	44.70	1.00	20.88
0.01	0.55	0.50	0.02	70.70	1.00	19.08
0.01	0.55	0.80	0.0125	89.40	1.00	15.21
0.01	0.55	0.10	0.10	31.60	1.00	21.13
0.01	0.55	0.10	0.50	31.60	5.00	21.13
0.01	0.55	0.10	1.00	31.60	10.00	21.13

ing C_F results in the displacement of the maximum axial velocity towards the wall. The secondary flow is also reduced for larger Forchheimer coefficients (which physically corresponds to larger resistance to the flow by the porous medium), as shown in the vector plots of the secondary flow. The displacement of the maximum value of the dimensionless temperature from the center to the wall becomes smaller with the increase of C_F, however, the value of the maxi-

mum increases, opposite to the axial velocity. The Nusselt number also increases, as shown in Table 1. When C_F increases from zero (this assumption means that the form drag due to the solid obstacles in the porous medium is totally ignored) to 0.25, the change is much larger than when it increases from 0.25 to 0.5, for both the velocity and the temperature.

The Dean number is a parameter used to characterize the magnitude and the shape of the secondary flow. The effect of the Dean number on the flow and heat transfer is investigated in Figs. 6–8. Fig. 6 shows that when *Dn* increases, the contour lines corresponding to large values of the axial velocity are displaced to the outer wall due to the centrifugal force and the value of the maximum axial velocity increases. The secondary flow also becomes stronger. Fig. 7 shows the contour lines of the dimensionless temperature for the corresponding Dean number. The maximum of the temperature is also displaced to the outer wall with the increase of the Dean number. The profile plots of the axial velocity and temperature in Fig. 8 show that the trends are similar except that the profile of the axial velocity is closer to that of a slug flow while the profile of the dimensionless temperature looks more as a deformed parabolic profile. Table 1 shows that the Nusselt number decreases when the Dean number is increased. It can be concluded that the Dean number has significant effect on the axial velocity, secondary flow, and heat transfer.

When the Darcy number, the Forchheimer coefficient, and the Dean number are fixed, the distributions of the axial velocity and temperature at the cross-section of a helical pipe do not show any significant sensitivity to the Germano number, which describes the effect of torsion on a flow in a helical pipe (Fig. 9). The Nusselt number remains the same, as seen from Table 1. However, the secondary flow does change, as seen from the contour lines of the stream function, which shows that the shape of the swirl is different for different values of the Germano number. It seems that the Germano number only affects the secondary flow but not the axial velocity and heat transfer.

5. Conclusions

This paper studies the laminar flow and heat transfer in a helical pipe filled with a fluid saturated porous medium for a constant wall heat flux. A full momentum equation that accounts for the Brinkman and Forchheimer extensions of the Darcy law and the flow inertia is utilized and derived in an orthogonal helical coordinate system. The effects of the parameters characterizing the porous medium, the Darcy number, *Da*, and the Forchheimer coefficient, C_F, and the parameters characterizing the helical pipe flow, the Dean number, *Dn*, and the Germano number, *Gn*, are investigated. Increasing the Darcy number results in a larger maximum value of the axial filtration velocity and a stronger secondary flow but a smaller value of the maximum of the dimensionless temperature and the Nusselt number. When *Da* is fixed and the Forchheimer coefficient, C_F, is increased, the axial velocity decreases and the secondary flow becomes weaker, however, the values of the maximum dimensionless temperature and the Nusselt number increase. The change is especially apparent when C_F changes from zero to a non-zero value. For the same porous medium (i.e., when *Da* and C_F are fixed), when the Dean number increases, the maximum values of the dimensionless axial velocity and the dimensionless temperature increase and the secondary flow become stronger. The Nusselt number increases with the Dean number. The increase of the Germano number does not have any significant effect on the axial velocity and heat transfer but strengthens the secondary flow.

Acknowledgements

The authors gratefully acknowledge the support of this work by a USDA grant. Helpful discussions with Prof. K.P. Sandeep are greatly appreciated. The authors are indebted to the reviewers for their comments.

References

[1] D.A. Nield, A. Bejan, Convection in Porous Media, second ed., Springer, New York, 1999.
[2] W.R. Dean, Note on the motion of fluid in a curved pipe, Philos. Magazine 4 (1927) 208–223.
[3] M. Germano, On the effect of torsion on a helical pipe flow, J. Fluid Mech. 125 (1982) 1–8.
[4] M. Germano, The Dean equations extended to a helical pipe flow, J. Fluid Mech. 203 (1989) 289–305.
[5] S. Liu, J.H. Masliyah, Axially invariant laminar flow in helical pipes with a finite pitch, J. Fluid Mech. 251 (1993) 315–353.
[6] S. Liu, J.H. Masliyah, Developing convective heat transfer in helical pipes with finite pitch, Internat. J. Heat Fluid Flow 15 (1994) 66–74.
[7] T.J. Hüttl, Navier–Stokes solutions of laminar flows based on orthogonal helical coordinates, Numer. Methods Laminar Turbulent Flow 10 (1997) 191–202.
[8] T.J. Hüttl, Influence of curvature and torsion on turbulent flow in curved and helically coiled pipes, Internat. J. Heat Fluid Flow 21 (2000) 345–353.
[9] J.G. Pharoah, S. Litster, N. Djilali, Mass transfer enhancement in membrane separation–rotating vs. helical modules, in: CFD 2003, Vancouver, May 2003, pp. 28–30.
[10] K.P. Sandeep, C.A. Zuritz, V.M. Puri, Modeling non-Newtonian two-phase flow in conventional and helical-holding tubes, Internat. J. Food Sci. Technol. 35 (2000) 511–522.
[11] L. Cheng, A.V. Kuznetsov, Investigation of a laminar flow of a non-Newtonian fluid in a helical pipe, Internat. J. Appl. Mech. Engrg. 10 (2005) 21–37.
[12] M. Sankariah, Y.V.N. Rao, Analysis of steady laminar flow of an incompressible Newtonian fluid through curved pipes of small curvature, ASME Paper No. 72-WA/FE-19, 1972.
[13] S.V. Patankar, V.S. Pratap, D.B. Spalding, Prediction of laminar flow and heat transfer in helically coiled pipes, J. Fluid Mech. 62 (1974) 539–551.
[14] G. Yang, Z.F. Dong, M.A. Ebadian, Laminar forced convection in a helicoidal pipe with finite pitch, Internat. J. Heat Mass Transfer 38 (1995) 853–862.

[15] C.X. Lin, P. Zhang, M.A. Ebadian, Laminar forced convection in the entrance region of helical pipes, Internat. J. Heat Mass Transfer 40 (1997) 3293–3304.
[16] B. Zheng, C.X. Lin, M.A. Ebadian, Combined laminar forced convection and thermal radiation in a helical pipe, Internat. J. Heat Mass Transfer 43 (2000) 1067–1078.
[17] L. Cheng, A.V. Kuznetsov, Heat transfer in a laminar flow of a non-Newtonian fluid in a helical pipe, Internat. J. Transport Phenomena 6 (2004) 293–306.
[18] D.A. Nield, A.V. Kuznetsov, Forced convection in a helical pipe filled with a saturated porous medium, Internat. J. Heat Mass Transfer 47 (2004) 5175–5180.
[19] L. Cheng, A.V. Kuznetsov, Investigation of laminar flow in a helical pipe filled with a fluid saturated porous medium, European J. Mech. B Fluids 24 (2005) 338–352.
[20] S.V. Patankar, Numerical Heat Transfer and Fluid Flow, McGraw-Hill, New York, 1980.